Nano Research

Open Access

Research Article

Enhanced methanol production from photothermal CO_2 reduction via multilevel interface design

Hongmin Wang[1,2,3,§], Bo Shang[1,2,§], Chungseok Choi[1,2,4], Sungho Jeon[5], Yuanzuo Gao[1,2], Tyler Wang[2,6], Nia J. Harmon[1,2], Mengxia Liu[2,7], Eric A. Stach[5], and Hailiang Wang[1,2] ✉

[1] *Department of Chemistry, Yale University, New Haven, CT 06520, USA*
[2] *Energy Sciences Institute, Yale University, West Haven, CT 06516, USA*
[3] *Current address: School of Materials Science and Engineering, Southeast University, Nanjing 211189, China*
[4] *Current address: SKKU Advanced Institute of Nanotechnology and Department of Nanoengineering, Sungkyunkwan University, Suwon 16419, Republic of Korea*
[5] *Department of Materials Science and Engineering, University of Pennsylvania, Philadelphia, PA 19104, USA*
[6] *Department of Physics, Yale University, New Haven, CT 06511, USA*
[7] *Department of Electrical Engineering, Yale University, New Haven, CT 06511, USA*
[§] *Hongmin Wang and Bo Shang contributed equally to this work.*

Cite this article: *Nano Research*, **2025**, *18*, 94907160. https://doi.org/10.26599/NR.2025.94907160

ABSTRACT: Photothermal CO_2 hydrogenation is a promising route to produce methanol as a sustainable liquid solar fuel. However, most existing catalysts require a combination of solar irradiation and additional heat input to achieve a satisfactory reaction rate. For the few that can be driven solely by light, their reaction rates are one order of magnitude lower. We develop a photothermal catalyst with multilevel interfaces that achieves improved methanol production from photothermal CO_2 hydrogenation without external heat. The catalyst features a layered structure comprising Cu/ZnO/Al_2O_3 (CZA) covered by oxidized carbon black (oCB), where the oCB/CZA interface promotes efficient heat generation and transfer, and the Cu/oxide interface contributes to high catalytic activity. Under a mild pressure of 8 bar, our oCB/CZA catalyst shows a methanol selectivity of 64.7% with a superior production rate of 4.91 mmol·g_{cza}^{-1}·h^{-1}, at least one order of magnitude higher than other photothermal catalysts solely driven by light. This work demonstrates a photothermal catalyst design strategy for liquid solar fuel production.

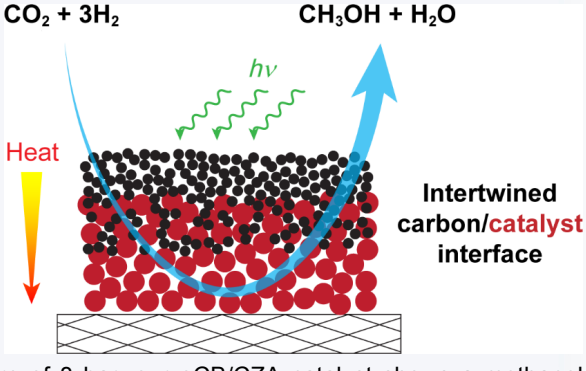

KEYWORDS: photothermal catalysis, CO_2 hydrogenation, methanol production, solar fuel, multilevel interface, Cu/ZnO/Al_2O_3 (CZA) catalyst

Methanol is an important feedstock for about 30% of industrial chemicals and a liquid fuel with an energy density of 15.9 MJ·L^{-1} [1, 2]. The industrial production of methanol relies on the thermocatalytic reaction between CO and H_2 which involves fossil fuel feedstocks and high temperature (> 200 °C) and pressure (> 50 bar) reaction conditions, causing massive energy consumption and carbon footprints [3]. To enable sustainable and distributed methanol production, it would be desirable to use emitted CO_2 and green H_2 as reactants and replace the thermal input with solar energy [1, 2]. Photothermal CO_2 hydrogenation could be such a route. Compared to conventional photochemical reactions, photothermal reactions can achieve much higher rates due to elevated temperatures and facile light-mediated kinetics [1]. However, most photothermal catalysts require external heat to drive the reaction, while light mainly serves as a secondary stimulus to lower activation energy and promote reaction rates [4–15]. Up to now, only In-based catalysts have been reported to show activity for methanol formation under illumination without additional heat input [16, 17]. Nevertheless, this process is limited by In's scarcity in the Earth's crust [18] and low methanol production rate at the μmol·g_{cat}^{-1}·h^{-1} scale.

Catalysts with designed interfacial structures may promote

Received: November 4, 2024; **Revised:** November 26, 2024
Accepted: November 26, 2024

✉Address correspondence to hailiang.wang@yale.edu

product selectivity [19] and reaction rate [20] of CO_2 reduction reactions. Our previous work demonstrated photothermal CO_2 hydrogenation to CO without external heat with a lotus-pod-structured Co/C catalyst prepared by pyrolyzing Co salt-impregnated cotton where the porous C support converts solar irradiation to heat and the Co nanoparticles catalyze the chemical reaction [21]. Potentially, this catalyst structure design can be applied to enable photothermal production of methanol from CO_2. However, most of the known catalysts for CO_2 hydrogenation to methanol are not compatible with the 900 °C pyrolysis temperature that we used to prepare the Co/C catalyst [22]. To extend the design of carbon/catalyst interfaces to photothermal methanol production, new catalyst architectures and their preparation methods are yet to be developed.

In this work, we developed a layer-structured photothermal catalyst with multilevel interfaces that can effectively convert CO_2 to methanol under illumination without external heat. The catalyst contains an oxidized carbon black (oCB) layer on the top, a $Cu/ZnO/Al_2O_3$ (CZA) layer in the middle, and a glass fiber paper (GFP) support layer at the bottom (Fig. 1). During operation, oCB converts light to heat and transfers heat to CZA which catalyzes CO_2 hydrogenation at its metal/oxide interface. The partially oxidized carbon surface promotes polar interaction with CZA, contributing to an intertwined oCB/CZA interface with enhanced heat transfer [6]. Under a mild pressure of 8 bar with 2.8 W·cm^{-2} illumination, our photothermal catalyst shows a superior methanol production rate of 4.91 mmol·g_{CZA}^{-1}·h^{-1} with 65% selectivity. This rate is equivalent to that of a typical thermal catalyst [23] and at least one order of magnitude higher than other catalysts solely driven by light [16, 17].

The CZA catalyst was prepared from thermal H_2 reduction of a $CuO/ZnO/Al_2O_3$ precursor which was prepared via co-precipitation and calcination (see the Electronic Supplementary Material (ESM) for details). The powder X-ray diffraction (XRD) pattern of as-synthesized $CuO/ZnO/Al_2O_3$ shows peaks corresponding to monoclinic CuO, wurtzite ZnO, and γ-Al_2O_3 (Fig. 2(a)). Scanning electron microscopy (SEM) images and energy-dispersive X-ray (EDX) maps show ~ 60 nm-sized Cu-containing particles distributed in a matrix containing Zn and Al (Fig. S1 in the ESM). After reduction by H_2, the morphology remains the same (Fig. S2 in the ESM) while the XRD peaks corresponding to CuO are replaced by Cu peaks (Fig. 2(a)), indicating the formation of

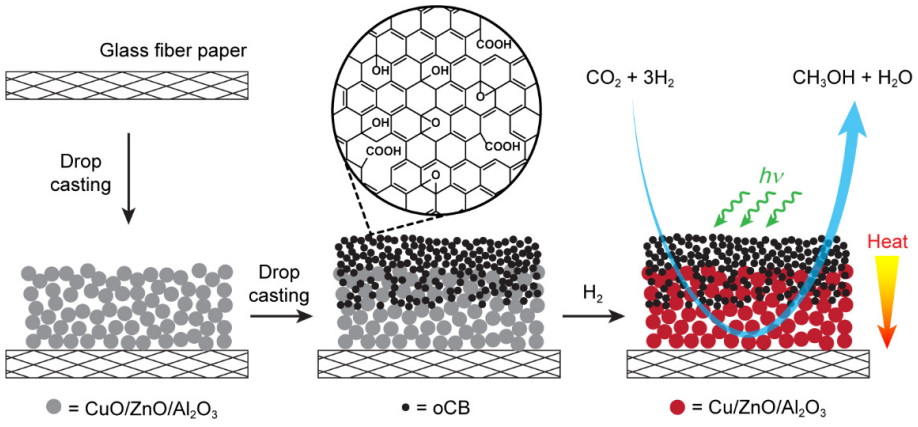

Figure 1 Schematic illustration of catalyst preparation and the layered structure for photothermal CO_2 hydrogenation to methanol.

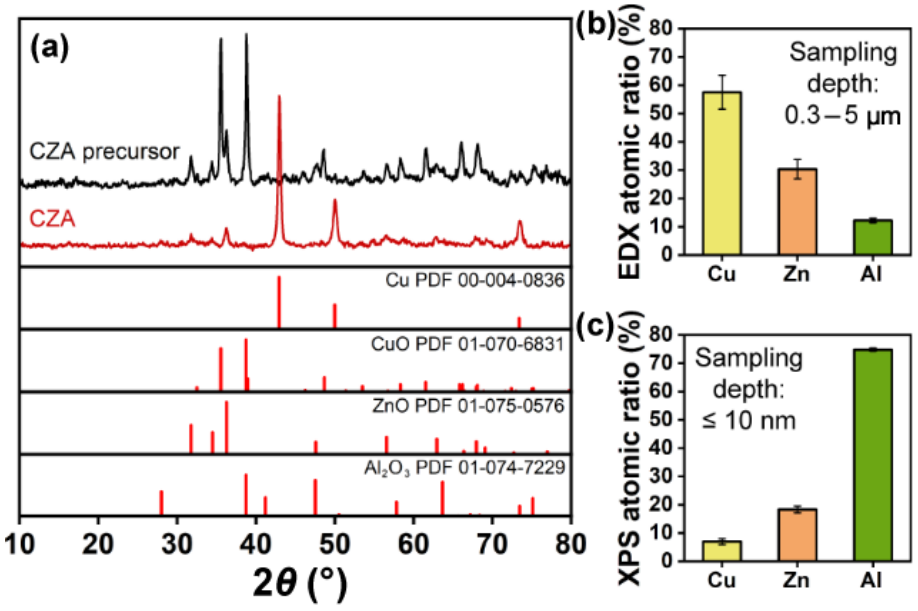

Figure 2 Structural characterization of the CZA catalyst. (a) XRD patterns of as-synthesized $CuO/ZnO/Al_2O_3$ precursor and H_2-reduced $Cu/ZnO/Al_2O_3$ catalyst. Atomic ratios of Cu, Zn, and Al obtained from (b) EDX and (c) XPS.

CZA. EDX spectroscopy of CZA with a 0.3–5 μm sampling depth confirms the existence of Cu, Zn, Al, and O (Fig. S3 in the ESM) with an atomic ratio of Cu:Zn:Al = 6:3:1 (Fig. 2(b)), the same as the input ratio in the synthesis. Inductively coupled plasma mass spectrometry analysis of CZA shows a similar atomic ratio of Cu:Zn:Al = 6.7:2.7:0.6. X-ray photoelectron spectroscopy (XPS) with a sampling depth ≤ 10 nm shows a different atomic ratio of Cu:Zn:Al = 1:2:7 (Fig. 2(c) and Fig. S4 in the ESM), indicating that the catalyst surface is relatively poor in Cu and rich in oxide. The Cu/oxide interface has been reported to be important for dispersing and stabilizing the Cu sites, straining the Cu lattice for high activity, and enabling a dual site mechanism for enhanced methanol production [6, 24, 25].

CZA materials are mostly known as the industrial catalyst with a specific surface area of 60–100 $m^2 \cdot g^{-1}$ for thermochemical methanol production from CO_2 hydrogenation [3, 25–27]. In the most widely accepted reaction mechanism, Cu adsorbs and disassociates H_2, ZnO stabilizes CO_2-derived intermediates, and Al_2O_3 adjusts the reducibility of ZnO and provides a high surface area for dispersing the Cu sites [6, 24, 25, 27]. In this work, the known plasmonic effect and photothermal response of Cu [28] inspired us to test CZA for photothermal CO_2 hydrogenation without external heat. Indeed, the ultraviolet–visible–near infrared (UV–vis–NIR) absolute reflectance spectrum of CZA shows strong light absorption with ~ 5% UV–vis reflectance and ~ 20% NIR reflectance (Fig. S5 in the ESM). To test the catalytic performance, the $CuO/ZnO/Al_2O_3$ precursor was dispersed in ethanol, drop-casted on a GFP support, and then reduced in H_2 to form CZA (Fig. S6 in the ESM). When the catalyst mass loading is 10 $mg \cdot cm^{-2}$, CZA gives a surface temperature of 289 °C under 2.8 $W \cdot cm^{-2}$ Xe lamp illumination (Fig. S7 in the ESM), sufficient to initiate CO_2 hydrogenation [3, 26]. The Xe lamp was utilized to simulate concentrated sunlight, which in practical application could be replaced by a focusing lens under natural sunlight [21]. The catalysis was performed in a batch reactor filled with H_2 and CO_2 (3:1 by partial pressure) at a total pressure of 8 bar with 2.8 $W \cdot cm^{-2}$ illumination (Fig. S8 in the ESM, default reaction condition). We adopted this relatively low reaction pressure to study the reaction for its compatibility with low-pressure (< 20 bar) CO_2/H_2 sources generated from renewable processes such as solar water splitting or biomass reforming [29]. CO and methanol were the only reduction products detected by gas chromatography (Fig. S9 in the ESM) and ^1H nuclear magnetic resonance (NMR) (Fig. S10 in the ESM). CZA with the mass loading of 10 $mg \cdot cm^{-2}$ shows a methanol production rate of 1.86 $mmol \cdot g_{cza}^{-1} \cdot h^{-1}$ with 62.9% selectivity in a 30 min reaction (Fig. S11 in the ESM). Mass loadings other than 10 $mg \cdot cm^{-2}$ lead to lower methanol production rates, possibly due to insufficient light-to-heat conversion at low mass loadings and mechanically unstable catalyst films with cracks at high mass loadings (Fig. S11(a) in the ESM). Therefore, we selected 10 $mg \cdot cm^{-2}$ as the optimized CZA mass loading for the following studies.

In order to enhance light-to-heat conversion, we tried depositing a carbon layer on top of the CZA precursor before reducing it in H_2. When carbon nanotubes are used to prepare this structure, the carbon layer cracks and falls apart after it is dried (Fig. S12 in the ESM) possibly due to the entanglement of nanotubes that intensifies structural deformation during solvent evaporation. Without entanglement, the use of spherical Super-P carbon black (CB, a specific surface area of 62 $m^2 \cdot g^{-1}$) nanoparticles leads to a uniform and mechanically stable carbon layer (Fig. S12 in the ESM). SEM images and EDX maps reveal a laminar structure composed of a layer of ~ 50 nm-sized CB particles on top, CZA particles in the middle, and the GFP support at the bottom, with a sharp flat CB/CZA interface (Fig. S13 in the ESM). UV–vis–NIR absolute reflectance spectrum of CB/CZA shows enhanced NIR absorption with CB coating on CZA (Fig. S5 in the ESM). The CB/CZA catalyst containing 0.5 $mg \cdot cm^{-2}$ of CB and 10 $mg \cdot cm^{-2}$ of CZA delivers a surface temperature of 305 °C under 2.8 $W \cdot cm^{-2}$ illumination, 16 °C higher than the CZA-only catalyst (Fig. S7(b) in the ESM).

We highlight the advantage of the CB/CZA layered structure by comparing it with a CB + CZA mixed structure prepared from casting a mixture of CB and CZA. At 0.5 $mg \cdot cm^{-2}$ of CB mass loading, the surface color of the layered CB/CZA is as black as CB (Fig. 3(a)), indicating strong light absorption. The color of the mixed CB + CZA appears to be the same as CZA, almost unaffected by the 5 wt.% carbon addition (Fig. 3(a) and Fig. S11(a) in the ESM). Under the default reaction condition, the CB/CZA catalyst shows a methanol production rate of 2.93 $mmol \cdot g_{cza}^{-1} \cdot h^{-1}$ with 60% selectivity, much higher than CZA (Fig. S11 in the ESM) or CB + CZA (Fig. 3(a)). CB + CZA shows even lower activity than CZA alone, possibly due to carbon blocking active catalytic sites. For CB/CZA, the methanol production rate increases with the CB mass loading until 0.75 $mg \cdot cm^{-2}$ at which the carbon layer cracks (Fig. 3(b)). Therefore, we determined 0.5 $mg \cdot cm^{-2}$ to be the optimal CB loading.

The effects of light intensity, reaction pressure, and reaction time on catalytic performance were further investigated with the layered CB/CZA catalyst. The light intensity controls the catalyst's surface temperature (Fig. S7(b) in the ESM) and thus influences the methanol production rate. Note that while the measured temperatures are likely subject to certain errors, they are still overall consistent with values measured by a different method (Fig. S14 in the ESM). When the light intensity is increased stepwise from 1.5 to 2.8 $W \cdot cm^{-2}$, the methanol production rate increases from 0.21 to 2.93 $mmol \cdot g_{cza}^{-1} \cdot h^{-1}$ with a relatively constant selectivity of ~ 60% (Fig. 3(c)). The unchanged selectivity indicates that within this light intensity range the reaction is controlled by kinetics instead of thermodynamics, as high temperature thermodynamically favors the endothermic CO formation reaction ($\Delta H°$ = +39 $kJ \cdot mol^{-1}$) instead of the exothermic methanol formation reaction ($\Delta H°$ = −50 $kJ \cdot mol^{-1}$) [3]. Correlating reaction rate with temperature leads to an Arrhenius plot showing a reasonably good linear correlation (Fig. S15 in the ESM). The apparent activation energy is calculated to be 77.1 $kJ \cdot mol^{-1}$, close to the value of ~ 70 $kJ \cdot mol^{-1}$ measured for Cu-based catalysts in thermocatalytic CO_2 hydrogenation to methanol [27, 30]. This match suggests that the contribution from photon-mediated reaction is insignificant in our system. When the total pressure is increased stepwise from 4 to 12 bar, the methanol production rate barely changes whereas the selectivity increases from 23% to 77% (Fig. 3(d)). The increased methanol selectivity at higher pressure is due to Le Chatelier's principle, namely high pressure favoring the pressure-reducing methanol formation reaction ($CO_2 + 3H_2 \rightarrow CH_3OH + H_2O$) over the pressure-maintaining reverse water–gas shift competing reaction ($CO_2 + H_2 \rightarrow CO + H_2O$) [1, 3]. The CB/CZA catalyst is stable in its performance for 3 h, as indicated by the maintained methanol production rate and selectivity (Fig. 3(e)).

However, as the reaction is extended beyond 3 h, the methanol production rate and selectivity of the CB/CZA catalyst considerably

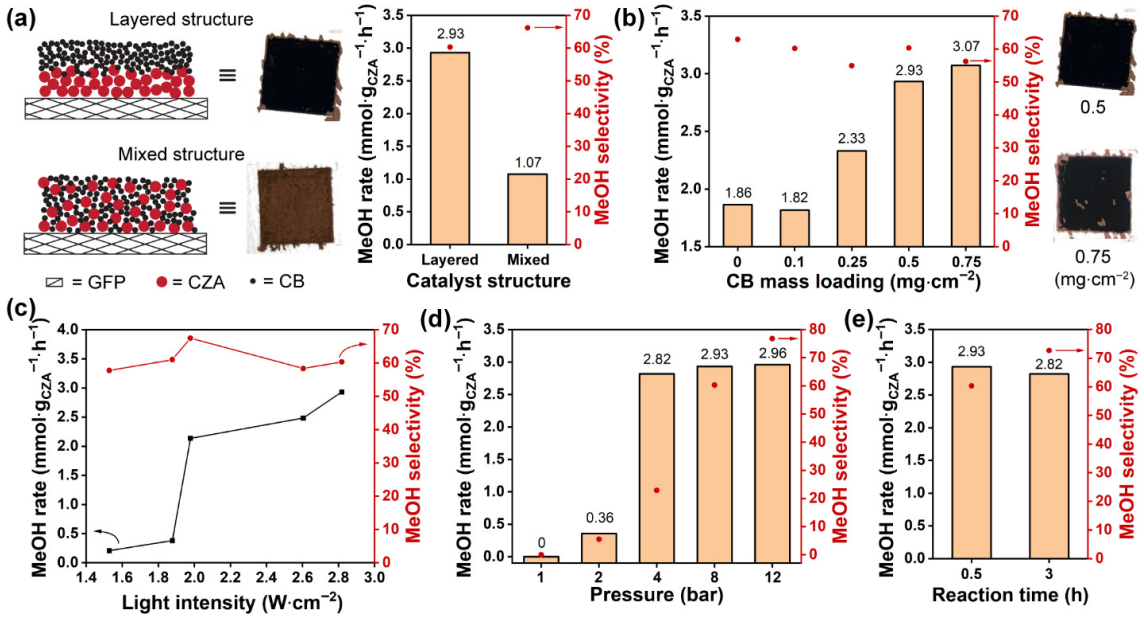

Figure 3 Photothermal CO_2 hydrogenation performance of the CB/CZA catalyst. (a) Comparison in structure and catalytic performance between CB/CZA and CB + CZA. (b) Effect of CB mass loading on structural stability and catalytic performance. Catalytic performance with varying (c) light intensity, (d) reaction pressure, and (e) reaction time.

decreases (Figs 4(a) and 4(b)). This performance decay is likely due to catalyst deactivation rather than the reaction reaching its thermodynamic equilibrium, as the CO_2 conversion remains below 10% (Fig. 4(a)). Therefore, we chose a catalyst after 12 h of reaction for post-mortem structural analysis. Cu 2p core-level XPS shows a peak shift from 932.1 to 935.2 eV, suggesting surface oxidation of Cu(0) to Cu(II) (Fig. 4(c)). This is possibly due to Cu reacting with H_2O accumulated as a product in the batch reactor [31]. The atomic ratio of Cu to all metals decreases by approximately a half (Fig. 4(d)), suggesting a decrease of Cu coverage on the catalyst surface. The atomic ratio of oxygen to all metals roughly doubles after the reaction (Fig. 4(e)), which is in line with the observed oxidation/hydration and Cu shrinkage on the surface. High-angle annular dark-field scanning transmission electron microscopy (HAADF-STEM) images and EDX maps of the CZA in CB/CZA before and after reaction show Cu particle size increase from ~ 50 to > 200 nm along with particle shape change from granular to irregular (Figs. 4(f) and 4(g), and Fig. S16 in the ESM). SEM images and EDX maps also confirm the significant increase in Cu particle size from ~ 60 to > 200 nm after the reaction (Fig. S17 in the ESM). Taking the results together, we conclude that the catalyst deactivation is caused by surface oxidation and Cu sintering, which agrees with Refs. [24, 25].

Since the CB/CZA interface plays an essential role in the

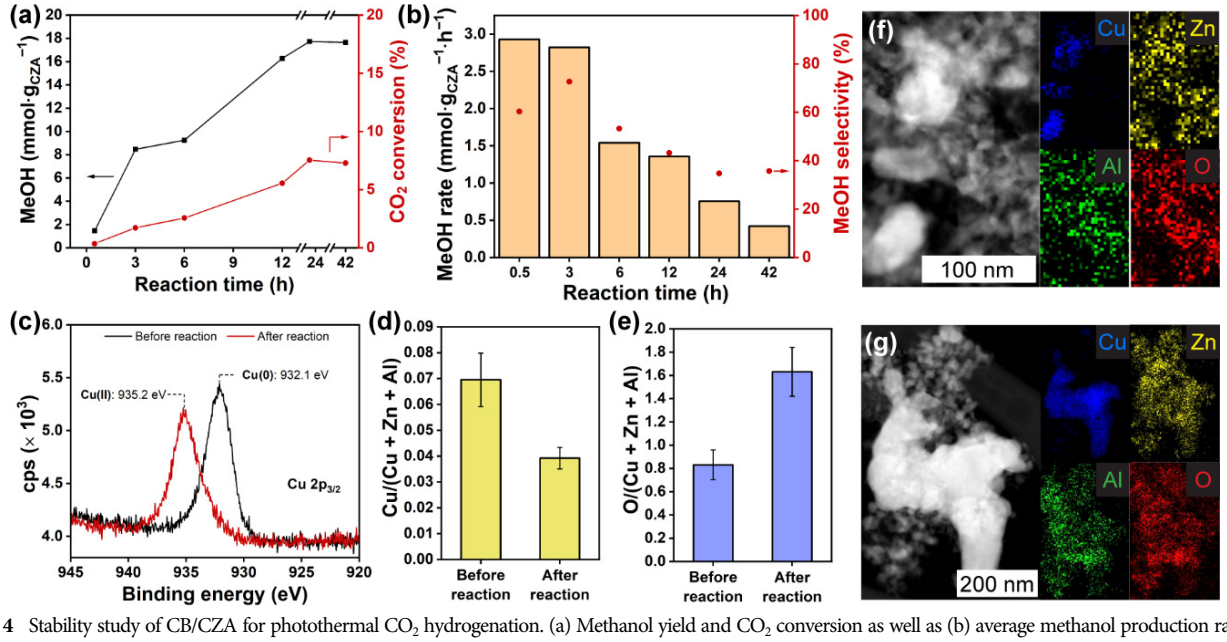

Figure 4 Stability study of CB/CZA for photothermal CO_2 hydrogenation. (a) Methanol yield and CO_2 conversion as well as (b) average methanol production rate with selectivity for different reaction durations. (c) Cu $2p_{3/2}$ core level XPS before and after 12 h of reaction. Atomic ratios of (d) Cu and (e) O over total metal elements measured by XPS for the catalyst before and after 12 h of reaction. STEM images and EDX maps of the catalyst (f) before and (g) after 12 h of reaction.

photothermal catalysis, we further considered functionalization of the carbon surface to enhance its interaction with CZA for improved heat transfer. To this aim, we oxidized CB using $KMnO_4$, $NaNO_3$, and H_2SO_4 (see the ESM for details). SEM image of the resulting partially oxidized CB (oCB) reveals ~ 50 nm-sized spherical particles (Fig. S18 in the ESM), identical to pristine CB. oCB/CZA catalysts were prepared following the same procedure as for CB/CZA. Cross-section SEM images and EDX maps of oCB/CZA show an intertwined carbon/CZA interface with oCB particles protruding into the CZA layer (Fig. S18 in the ESM), as opposed to the sharp flat interface in CB/CZA (Figs. 5(a) and 5(b)). This structural difference is likely caused by the polar interaction between oCB and CZA.

Under the default reaction condition, the oCB/CZA photothermal catalyst containing 0.5 mg·cm^{-2} of oCB and 10 mg·cm^{-2} of CZA shows a methanol production rate of 4.91 mmol·g_{cza}^{-1}·h^{-1} with 65% selectivity in a 30 min reaction (Fig. 5(c)). oCB mass loadings other than 0.5 mg·cm^{-2} lead to lower methanol production rates (Fig. 5(d)). Note that oCB/CZA was pre-treated in H_2 at 350 °C for 30 min to avoid decarboxylation or hydrogenation of oCB during the photothermal catalysis. To confirm that the methanol is formed from CO_2 hydrogenation instead of oCB decomposition, we performed control experiments utilizing pure H_2 or CO_2 as reactant gas. Gas chromatography and ^{1}H NMR show an absence of CO and methanol unless both H_2 and CO_2 are present, demonstrating CO_2, not oCB, as the carbon source for the reaction (Figs. S9 and S10 in the ESM). The methanol production rate and selectivity achieved by our oCB/CZA catalyst are much higher than those reported for other photothermal catalysts solely driven by light [16, 17], and are superior to the state-of-the-art catalysts simultaneously driven by light and heat (Fig. 5(e) and Table S1 in the ESM) [4, 5, 7, 9, 11–15]. The catalytic performance of oCB/CZA is also comparable to that of CZA catalysts tested under thermochemical conditions [23], demonstrating relatively efficient light-to-heat conversion and heat transfer in our catalyst system. The similarity in methanol production rate between photothermal and thermal reactions, together with their similar apparent activation energy values (Fig. S15 in the ESM), suggests that our reaction is dominated by the photothermal pathway with little influence from photochemical effects. This conclusion agrees with a previous report on a similar CZA catalyst that the rate of methanol production increased by only 5% when light was introduced at temperatures above 250 °C [6].

To investigate the origin of oCB/CZA's high catalytic performance, we compare light absorption and photothermal conversion properties between CB and oCB. UV–vis–NIR absolute reflectance spectroscopy measurements of CB/CZA and oCB/CZA show similar reflectance of ~ 5% in the entire wavelength range (Fig. S5 in the ESM). Consistently, CB and oCB exhibit similar temperatures under the same illumination (Fig. S14 in the ESM), indicating their equivalent light-to-heat conversion capability. The similarity in both light-to-heat conversion and optical properties between CB/CZA and oCB/CZA leaves the interfacial structure and heat transfer the most probable reason for the improved catalytic activity of oCB/CZA compared to CB/CZA. We simulated heat transfer through the oCB/CZA vs. CB/CZA interfaces using COMSOL (see the ESM for details). A simplified interdigitated interface structure was adopted to represent the intertwined oCB/CZA interface. After the carbon surfaces reach the same temperature as measured by our experiments (Fig. S7(b) in the ESM) under identical illumination conditions, the bulk phase of the

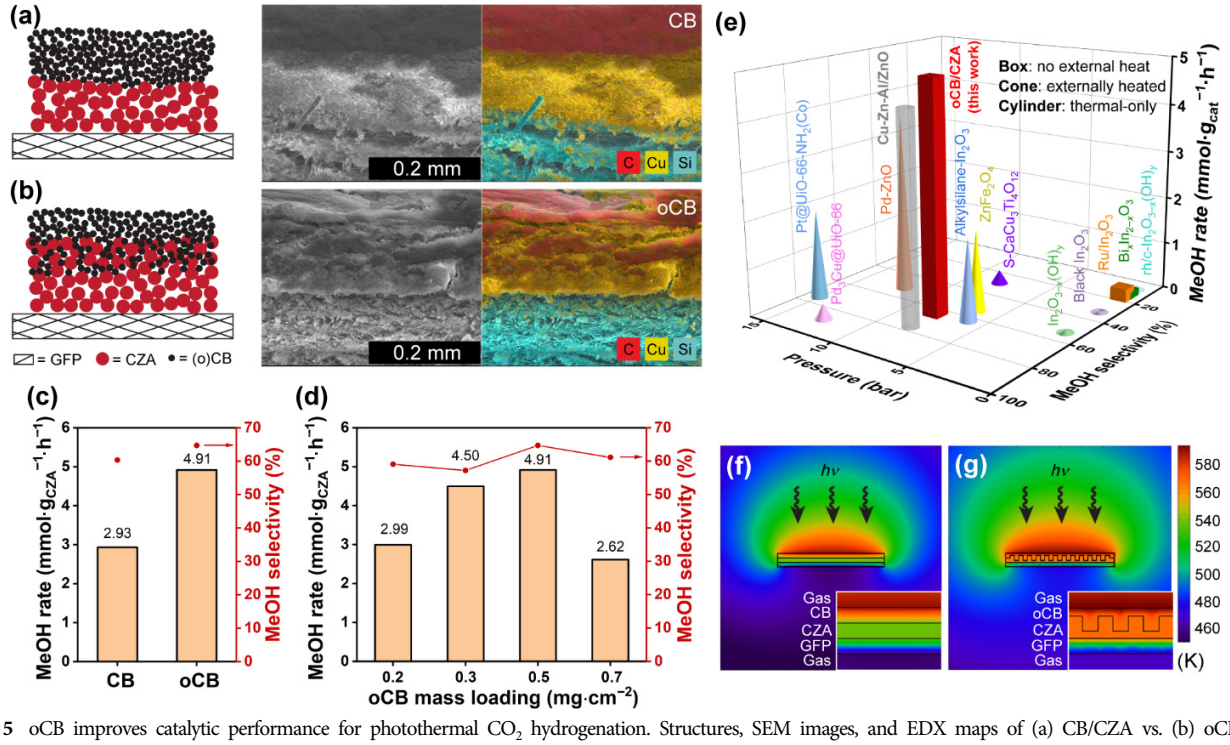

Figure 5 oCB improves catalytic performance for photothermal CO_2 hydrogenation. Structures, SEM images, and EDX maps of (a) CB/CZA vs. (b) oCB/CZA interfaces. (c) Catalytic performance comparison between CB/CZA and oCB/CZA under default reaction condition. (d) Effect of oCB mass loading on methanol production rate and selectivity. (e) Comparison in activity, selectivity, and reaction pressure of oCB/CZA with other methanol-producing photothermal and thermal CO_2 hydrogenation catalysts. Detailed reaction conditions are summarized in Table S1 in the ESM. Modeling of temperature distribution near (f) the CB/CZA catalyst with a flat interface vs. (g) the oCB/CZA catalyst with an intertwined interface.

interdigitated CZA is 50 °C hotter than the flat CZA (Figs. 5(f) and 5(g)). This higher temperature originates from the increased contact area that improves heat transfer from the top carbon layer as a light-to-heat converter to the underneath CZA catalyst layer as a heat receiver. The enhanced heat transfer in oCB/CZA enhances methanol production and improves energy utilization, but does not alter methanol selectivity as compared to CB/CZA (Fig. 5(c)), indicating that the reaction is kinetically controlled, which is in line with the results from the light intensity study (Fig. 3(c)).

The stability of oCB/CZA catalyzing photothermal CO_2 hydrogenation was characterized by a several-cycle test in which we manually reset the reaction every 4 h. The methanol production rate for the last cycle is 65% of that for the first cycle (Fig. S19 in the ESM). This reasonable durability demonstrates that water vapor buildup may be an important factor for catalyst deactivation which can be effectively mitigated by intermittently resetting the reactant gas. Future work may continue to advance this reaction by exploring catalysts with higher chemical and physical tolerance than CZA and by changing to a flow reactor for timely product removal.

In summary, we have developed an oCB/CZA catalyst with superior activity towards photothermal CO_2 hydrogenation to generate methanol. The oCB component and its intertwined interface with CZA enable effective light-to-heat conversion and heat transfer, and the Cu/oxide interface provides catalytically active sites for the CO_2 reduction reaction. This work provides a strategy for converting industrial thermal catalysts into photothermal catalysts for solar fuel production.

Electronic Supplementary Material: Supplementary material (experimental and modeling details, and additional characterization and reaction results) is available in the online version of this article at https://doi.org/10.26599/NR.2025.94907160.

Data availability

All data needed to support the conclusions in the paper are presented in the manuscript and the Electronic Supplementary Material. Additional data related to this paper may be requested from the corresponding author upon request.

Acknowledgments

This work was solely supported by the Center for Hybrid Approaches in Solar Energy to Liquid Fuels (CHASE), an Energy Innovation Hub funded by the U.S. Department of Energy, Office of Science, Office of Basic Energy Sciences under Award Number DE-SC0021173. The electron microscopy was carried out at the Singh Center for Nanotechnology, which was supported by the NSF National Nanotechnology Coordinated Infrastructure Program under grant NNCI-2025608. Additional support to the Nanoscale Characterization Facility at the Singh Center has been provided by the Laboratory for Research on the Structure of Matter (MRSEC) supported by the National Science Foundation (DMR-1720530).

Declaration of competing interest

Hailiang Wang is an associate editor of this journal, but he is not involved in the peer-review or decision of this article. The other contributing authors report no conflict of interests in this work.

Author contribution statement

H. M. W.: Conceptualization, investigation, writing. B. S.: Investigation. C. C.: Investigation. S. J.: Investigation. Y. Z. G.: Investigation. T. W.: Investigation. N. J. H.: Investigation. M. X. L.: Resources. E. A. S.: Resources. H. L. W.: Conceptualization, project administration, writing. All the authors have approved the final manuscript.

Use of AI statement

None.

References

[1] Tountas, A. A.; Peng, X. Y.; Tavasoli, A. V.; Duchesne, P. N.; Dingle, T. L.; Dong, Y. C.; Hurtado, L.; Mohan, A.; Sun, W.; Ulmer, U. et al. Towards solar methanol: Past, present, and future. *Adv. Sci.* **2019**, *6*, 1801903.

[2] Zhang, Z. S.; Ding, X.; Yang, X. G.; Tu, W. G.; Wang, L.; Zou, Z. G. Shedding light on CO_2: Catalytic synthesis of solar methanol. *EcoMat* **2021**, *3*, e12078.

[3] Sheldon, D. Methanol production—A technical history. *Johnson Matthey Technol. Rev.* **2017**, *61*, 172–182.

[4] Wang, L.; Ghoussoub, M.; Wang, H.; Shao, Y.; Sun, W.; Tountas, A. A.; Wood, T. E.; Li, H.; Loh, J. Y. Y.; Dong, Y. C. et al. Photocatalytic hydrogenation of carbon dioxide with high selectivity to methanol at atmospheric pressure. *Joule* **2018**, *2*, 1369–1381.

[5] Wu, D. D.; Deng, K. X.; Hu, B.; Lu, Q. Y.; Liu, G. L.; Hong, X. L. Plasmon-assisted photothermal catalysis of low-pressure CO_2 hydrogenation to methanol over Pd/ZnO catalyst. *ChemCatChem* **2019**, *11*, 1598–1601.

[6] Xie, B. Q.; Wong, R. J.; Tan, T. H.; Higham, M.; Gibson, E. K.; Decarolis, D.; Callison, J.; Aguey-Zinsou, K. F.; Bowker, M.; Catlow, C. R. A. et al. Synergistic ultraviolet and visible light photo-activation enables intensified low-temperature methanol synthesis over copper/zinc oxide/alumina. *Nat. Commun.* **2020**, *11*, 1615.

[7] Yan, T. J.; Li, N.; Wang, L. L.; Liu, Q.; Ali, F. M.; Wang, L.; Xu, Y. F.; Liang, Y.; Dai, Y.; Huang, B. B. et al. How to make an efficient gas-phase heterogeneous CO_2 hydrogenation photocatalyst. *Energy Environ. Sci.* **2020**, *13*, 3054–3063.

[8] Xie, B. Q.; Kumar, P.; Tan, T. H.; Esmailpour, A. A.; Aguey-Zinsou, K. F.; Scott, J.; Amal, R. Doping-mediated metal–support interaction promotion toward light-assisted methanol production over $Cu/ZnO/Al_2O_3$. *ACS Catal.* **2021**, *11*, 5818–5828.

[9] Ling, L. L.; Yang, W. J.; Yan, P.; Wang, M.; Jiang, H. L. Light-assisted CO_2 hydrogenation over Pd_3Cu@UiO-66 promoted by active sites in close proximity. *Angew. Chem., Int. Ed.* **2022**, *61*, e202116396.

[10] Xie, B. Q.; Tan, T. H.; Kalantar-Zadeh, K.; Zheng, J. W.; Kumar, P.; Jiang, J. J.; Zhou, S. J.; Scott, J.; Amal, R. Promoting low-temperature methanol production over mixed oxide supported Cu catalysts: Coupling ceria-promotion and photo-activation. *Appl. Catal. B: Environ.* **2022**, *315*, 121599.

[11] Zhang, Z. S.; Mao, C. L.; Meira, D. M.; Duchesne, P. N.; Tountas, A. A.; Li, Z.; Qiu, C. Y.; Tang, S. L.; Song, R.; Ding, X. et al. New black indium oxide-tandem photothermal CO_2-H_2 methanol selective catalyst. *Nat. Commun.* **2022**, *13*, 1512.

[12] Chen, J. M.; Wang, Y. J.; Wang, F. L.; Li, Y. W. Photo-induced switching of CO_2 hydrogenation pathway towards CH_3OH production over Pt@UiO-66-NH_2(Co). *Angew. Chem., Int. Ed.* **2023**, *62*, e202218115.

[13] Jiang, Z. Y.; Yuan, Z. M.; Duchesne, P. N.; Sun, W.; Lyu, X.; Miao, W. K.; Viasus Pérez, C. J.; Xu, Y. F.; Yang, D. R.; Huang, B. B. et al. A living photocatalyst derived from $CaCu_3Ti_4O_{12}$ for CO_2

hydrogenation to methanol at atmospheric pressure. *Chem Catal.* **2023**, *3*, 100507.
[14] Lu, Z.; Xu, Y. F.; Zhang, Z. S.; Sun, J. C.; Ding, X.; Sun, W.; Tu, W. G.; Zhou, Y. F.; Yao, Y.; Ozin, G. A. et al. Wettability engineering of solar methanol synthesis. *J. Am. Chem. Soc.* **2023**, *145*, 26052–26060.
[15] Xu, Y. F.; Tountas, A. A.; Song, R.; Ye, J.; Wei, J. H.; Ji, S. F.; Zhao, L.; Zhou, W. Z.; Chen, J. H.; Zhao, G. S. et al. Equilibrium photothermodynamics enables a sustainable methanol synthesis. *Joule* **2023**, *7*, 738–752.
[16] Deng, B. W.; Song, H.; Wang, Q.; Hong, J. N.; Song, S.; Zhang, Y. W.; Peng, K.; Zhang, H. W.; Kako, T.; Ye, J. H. Highly efficient and stable photothermal catalytic CO_2 hydrogenation to methanol over Ru/In_2O_3 under atmospheric pressure. *Appl. Catal. B: Environ.* **2023**, *327*, 122471.
[17] Yan, T. J.; Li, N.; Wang, L. L.; Ran, W. G.; Duchesne, P. N.; Wan, L. L.; Nguyen, N. T.; Wang, L.; Xia, M. K.; Ozin, G. A. Bismuth atom tailoring of indium oxide surface frustrated Lewis pairs boosts heterogeneous CO_2 photocatalytic hydrogenation. *Nat. Commun.* **2020**, *11*, 6095.
[18] Lokanc, M.; Eggert, R.; Redlinger, M. *The Availability of Indium: The Present, Medium Term, and Long Term*; NREL/SR-6A20-62409; National Renewable Energy Laboratory: Golden, USA, 2015.
[19] Ning, S. B.; Ou, H. H.; Li, Y. G.; Lv, C. C.; Wang, S. F.; Wang, D. S.; Ye, J. H. Co^0–$Co^{\delta+}$ interface double-site-mediated C–C coupling for the photothermal conversion of CO_2 into light olefins. *Angew. Chem., Int. Ed.* **2023**, *62*, e202302253.
[20] Pan, W. Y.; Wei, Z. H.; Su, Y. H.; Lian, Y. B.; Zheng, Z. Y.; Yuan, H. H.; Qin, Y. Z.; Xie, X. L.; Bai, Q. Q.; Jiao, Z. Y. et al. Hydroxylated metal-organic-layer nanocages anchoring single atomic cobalt sites for robust photocatalytic CO_2 reduction. *Nano Res.* **2024**, *17*, 2410–2419.
[21] Wang, H. M.; Fu, S. T.; Shang, B.; Jeon, S.; Zhong, Y. R.; Harmon, N. J.; Choi, C.; Stach, E. A.; Wang, H. L. Solar-driven CO_2 conversion via optimized photothermal catalysis in a lotus pod structure. *Angew. Chem., Int. Ed.* **2023**, *62*, e202305251.
[22] Kung, H. H. Deactivation of methanol synthesis catalysts - a review. *Catal. Today* **1992**, *11*, 443–453.
[23] Du, S. C.; Tang, W. X.; Lu, X. X.; Wang, S. B.; Guo, Y. B.; Gao, P. X. Cu-decorated ZnO nanorod array integrated structured catalysts for low-pressure CO_2 hydrogenation to methanol. *Adv. Mater. Interfaces* **2018**, *5*, 1700730.
[24] Kamsuwan, T.; Guntida, A.; Praserthdam, P.; Jongsomjit, B. Differences in deterioration behaviors of $Cu/ZnO/Al_2O_3$ catalysts with different Cu contents toward hydrogenation of CO and CO_2. *ACS Omega* **2022**, *7*, 25783–25797.
[25] Behrens, M.; Studt, F.; Kasatkin, I.; Kühl, S.; Hävecker, M.; Abild-Pedersen, F.; Zander, S.; Girgsdies, F.; Kurr, P.; Kniep, B. L. et al. The active site of methanol synthesis over $Cu/ZnO/Al_2O_3$ industrial catalysts. *Science* **2012**, *336*, 893–897.
[26] Baltes, C.; Vukojevic, S.; Schuth, F. Correlations between synthesis, precursor, and catalyst structure and activity of a large set of $CuO/ZnO/Al_2O_3$ catalysts for methanol synthesis. *J. Catal.* **2008**, *258*, 334–344.
[27] Kunkes, E.; Behrens, M. Methanol chemistry. In *Chemical Energy Storage*. Schlögl, R., Ed.; De Gruyter: Berlin, 2013; pp 413–442.
[28] Xin, Y.; Yu, K. F.; Zhang, L. T.; Yang, Y. R.; Yuan, H. B.; Li, H. L.; Wang, L. B.; Zeng, J. Copper-based plasmonic catalysis: Recent advances and future perspectives. *Adv. Mater.* **2021**, *33*, 2008145.
[29] Davda, R. R.; Shabaker, J. W.; Huber, G. W.; Cortright, R. D.; Dumesic, J. A. A review of catalytic issues and process conditions for renewable hydrogen and alkanes by aqueous-phase reforming of oxygenated hydrocarbons over supported metal catalysts. *Appl. Catal. B: Environ.* **2005**, *56*, 171–186.
[30] Kipnis, M.; Volnina, E.; Belostotsky, I.; Galkin, R.; Zhilyaeva, N.; Levin, I.; Kottsov, S.; Ezhov, A. Effective $Cu/ZnO/Al_2O_3$ catalyst for methanol production: Synthesis, activation, catalytic performance, and regeneration. *Catal. Res.* **2022**, *2*, 27.
[31] Liang, B. L.; Ma, J. G.; Su, X.; Yang, C. Y.; Duan, H. M.; Zhou, H. W.; Deng, S. L.; Li, L.; Huang, Y. Q. Investigation on deactivation of $Cu/ZnO/Al_2O_3$ catalyst for CO_2 hydrogenation to methanol. *Ind. Eng. Chem. Res.* **2019**, *58*, 9030–9037.